Journal of Solid State Chemistry 182 (2009) 1492–1498

Contents lists available at ScienceDirect

Journal of Solid State Chemistry

journal homepage: www.elsevier.com/locate/jssc

B-site disordering in $Ba_3Ln_2MoO_9$ (Ln = Ho, Er) perovskites: A neutron diffraction study

S.A. Larrégola [a], J.A. Alonso [b], M. García Hernandez [b], M.T. Fernandez-Díaz [c], J.C. Pedregosa [a,*]

[a] Área de Química General e Inorgánica, Departamento de Química, Facultad de Química, Bioquímica y Farmacia, Universidad Nacional de San Luis, Chacabuco y Pedernera, 5700 San Luis, Argentina
[b] Instituto de Ciencia de Materiales de Madrid, C.S.I.C., Cantoblanco, 28049 Madrid, Spain
[c] Institut Max Von Laue Paul Langevin, F-38042 Grenoble, France

ARTICLE INFO

Article history:
Received 11 November 2008
Received in revised form
4 March 2009
Accepted 6 March 2009
Available online 24 March 2009

Keywords:
Barium perovskite
Neutron powder diffraction
X-ray powder diffraction
Joint Rietveld refinement
B-site disordering
Paramagnetic rare earth cations

ABSTRACT

We describe the preparation, structure determination and magnetic properties of two Ba perovskites containing rare-earth cations at the B-sublattice. $Ba_3Ln_2MoO_9$ (Ln = Ho^{3+} and Er^{3+}) were synthesized by ceramic procedures. Joint X-ray (XRPD) and neutron (NPD) powder diffraction refinements were carried out to analyse the crystal structure. At room temperature, both phases are tetragonal, space group $I4/mcm$, $Z = 4$. Ln and Mo atoms are found to be distributed at random over the octahedral sites of the perovskites. Magnetic measurements at 0.1 T show that both samples are paramagnetic between 3 and 300 K, following a Curie–Weiss law. M vs. H curves show a region of paramagnetic behaviour and above 2.5 T a magnetic saturated system is observed. Finally, the temperature evolution of the NPD patterns of $Ba_3Ho_2MoO_9$ reveals the absence of long-range magnetic ordering down to 2 K.

© 2009 Elsevier Inc. All rights reserved.

1. Introduction

The perovskite-type oxides have the general formula ABO_3; their crystal structure can be described as a framework of corner-sharing BO_6 octahedra which contains larger A cations at the voids in between them. Double perovskite-type oxides have the formula $A_2B'B''O_6$, where B' and B'' are different ions that can have different oxidation states. Many examples of compounds that present 1:1 long-range ordering over the six-coordinated B sites have been reported in the literature [1,2].

A particular type of double perovskites present the apparently complex stoichiometry $A_3B'_2B''O_9$ [3,4]. The crystallographic formula of these compounds could be re-written as $A_2B'(B_{1/3}'B_{2/3}'')O_6$ similar to $A_2B'B''O_6$ double perovskites. They, thus, display an intrinsic partial disordering over half of the perovskite ($B_{1/3}'B_{2/3}''$) positions.

It is well known that the physical properties of these compounds are strongly correlated with some structural factors, mainly, the order–disorder phenomena between the octahedral site atoms. The most important structural features that affect the long-range order of the B-cations are various and well known, such as the charge and ionic radii difference between B-site atoms and its electronic configuration, and the size ratio between A and B atoms [5,6]. In the same way, other alternative methods have been proposed to evaluate the order–disorder relationship in this kind of compounds [7,8].

Two different works have been reported on $A_3B'_2B''O_9$ double-perovskites containing rare-earth B' cations and hexavalent B'' cations. The first one, reported by Fuentes et al. [9], presents the synthesis and crystal structure of the double perovskites with A = Ba, B' = Dy, Sm and Gd; and B'' = W and Mo. The other report, given by Oyama et al. [10], reports a study of the crystal structure and the magnetic properties of the double perovskites $Ba_3Ln_2B''O_9$ with Ln = Nd–Lu and B'' = Mo and W. The only common sample of both studies, $Ba_3Dy_2MoO_9$, has been described as a cubic double perovskite in the first paper and as a monoclinic simple ABO_3 perovskite in the second one. Both works determine the crystal structures by X-ray powder diffraction. Due to the presence of so many strong scatterers, XRPD has a poor sensitivity to oxide anions in these kinds of compounds, so NPD techniques are preferred to correctly determine the oxygen positions, octahedral tilting and actual space group symmetry in these structures.

In order to solve the discrepancy existing between the structures reported for these oxides, we have chosen two double perovskites with Ln = Ho, Er, with rare-earth ions of similar size that Dy, but not presenting a very high neutron absorption cross section, to simplify the data acquisition and structural

* Corresponding author. Fax: +54 2652 430224.
E-mail address: jpedreg@unsl.edu.ar (J.C. Pedregosa).

0022-4596/$ - see front matter © 2009 Elsevier Inc. All rights reserved.
doi:10.1016/j.jssc.2009.03.008

determination. Due to the similitude of the neutron scattering lengths of the *Ln* ions used and Mo (8.0 fm and 7.7 fm for Ho and Er, respectively; and 6.7 fm for Mo) the crystal structures were analysed by a joint Rietveld refinement from high resolution XRPD and NPD data. The structural characterization of the perovskites $Ba_3Ho_2MoO_9$ (BHMO) and $Ba_3Er_2MoO_9$ (BEMO) has been completed with a study of their magnetic properties.

Finally, and in order to determine a possible magnetic ordering down to 1.8 K, we have carried out a sequential study of the thermal evolution of structure of one of these isostructural compounds in a high-flux neutron diffractometer.

2. Experimental

$Ba_3Ln_2MoO_9$ (Ln = Ho, Er) were obtained as well-crystallized brown powders by using solid-state techniques. As starting materials, $BaCO_3$, Ho_2O_3, Er_2O_3 and MoO_3 were used. They were weighed out in the appropriate metal ratios and well mixed in an agate mortar. The mixtures were calcined at 800 °C for 24 h. Subsequently, the products were treated two times at 1150 °C for 12 h with intermediate regrindings. Finally the samples were calcined at 1500 °C for 5 h until a single $Ba_3Ln_2MoO_9$ phase was obtained. The samples were slowly cooled within the furnace down to room temperature. All the calcination steps were carried out in platinum crucibles.

The initial structural identification and characterization of the samples was carried out by laboratory XRPD (Cu$K\alpha$, $\lambda = 1.5406$ Å). NPD data were collected at 295 K at the high-resolution powder diffractometer D1A. The high-flux mode was used, with a wavelength of 1.91 Å, selected from a Ge monochromator. About 4 g of sample were placed in a 8 mm diameter vanadium can; the counting time was 3 h. A study of the thermal evolution of the NPD patterns was carried out for the Ho sample in the D1B diffractometer between 1.8 and 275 K (ILL, Grenoble, France). High resolution XRPD diagrams were collected in a Rigaku MultiFlex diffractometer using the monochromatic Cu$K\alpha$ radiation in 2θ-steps of 0.02° and 5 s of counting time in the range $10° \leqslant 2\theta \leqslant 120°$.

The crystal structure determination for both samples was carried out from a joint Rietveld refinement of the high resolution XRPD and NPD data collected at RT, using the program Fullprof [11]. The following parameters were refined in the final run for both samples: scale factors, background coefficients, zero-point errors, pseudo-Voigt corrected for asymmetry parameters, positional coordinates, isotropic thermal factors, and occupancy factors for oxygen atoms. In the sequential refinement in the *I*4/*mcm* space group, the following parameters were varied: scale factor, *a* and *c* unit cell parameters, *x* and *y* atomic positions for O2 and an overall thermal factor; all the refinements were allowed to reach convergence. The neutron absorption of the rare earths was corrected with μr values of 0.308 and 0.126 for Er and Ho, respectively, estimated for the diameter of the sample cylinder.

The magnetic measurements were performed in a commercial superconducting quantum interference device magnetometer (SQUID). The magnetic susceptibility data were collected in the $3 < T < 300$ K range under an applied magnetic field of 0.1 T. Isothermal magnetization curves were obtained through magnetic fields of 5 T at $T = 3$ K.

3. Results

3.1. Crystal structure

The XRPD diagrams of $Ba_3Ln_2MoO_9$ (Ln = Ho, Er) shown in Figs. 1a and 2a are characteristic of a perovskite-type structure,

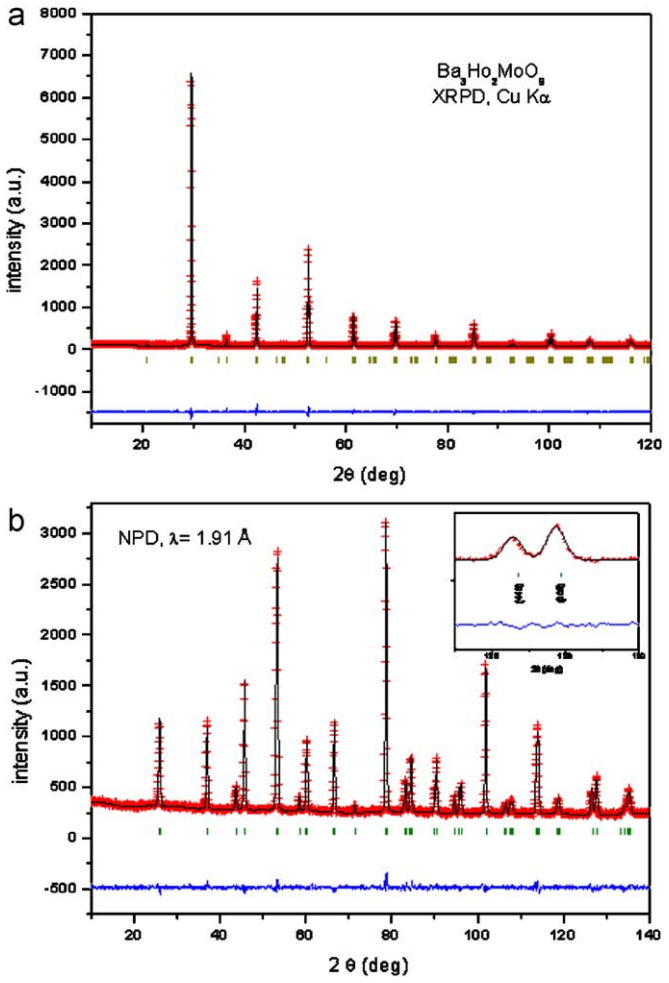

Fig. 1. Observed (circles), calculated (full line) and difference (bottom) profiles after a joint refinement for $Ba_3Ho_2MoO_9$: (a) XRPD fit part and (b). High resolution NPD at 295 K fit part. Inset: close up showing the tetrahedral splitting of (440) and (008) reflections.

which could be indexed in a tetragonal unit cell with parameters related to the ideal cubic perovskite parameter ($a_0 \approx 4$ Å) as $a = b \approx \sqrt{2}a_0$ and $c \approx 2a_0$. The insets of Figs. 1b and 2b correspond to the high angle region of the NPD patterns, showing the splitting of the reflections (440) and (008), characteristic of the tetragonal symmetry. A cubic symmetry with simple a_0 or doubled $2a_0$ parameter, as well as a rhombohedral symmetry, would not show this splitting. Many long-range ordered double perovskites with similar unit cell parameters have been described in the space group *I*4/*m* (no. 87). However, the absence of the reflections (110) and (113), characteristic of the long-range ordering of the *B* cations, suggests that *Ln* and Mo are fully disordered over the *B* positions. Therefore, the *I*4/*mcm* (no. 140) space group, describing the same tilting scheme $a^0a^0c^-$ [12] as *I*4/*m*, was successfully used to describe the structure. The observed reflection conditions (*hkl*: $h+k+l = 2n$; *h k* 0: $h+k = 2n$; 0 *k l*: *k*, $l = 2n$; *h h l*: $l = 2n$; 0 0 *l*: $l = 2n$; *h* 0 0: $h = 2n$) perfectly correspond to this space group. In the *I*4/*mcm* perovskite model it is necessary to define a single *A* and *B* positions and two different oxygen atoms. Ba atoms were placed at 4*b* (0, 1/2, 1/4) sites; *Ln* and Mo were randomly distributed over the 4*c* (0, 0, 0) sites; one of the oxygen atoms (O1) was located at the special 4*a* (0, 0, 1/4) site, whereas O2 is occupying the 8*h* (*x*, *x*+1/2, 0) position. The most important structural parameters of the

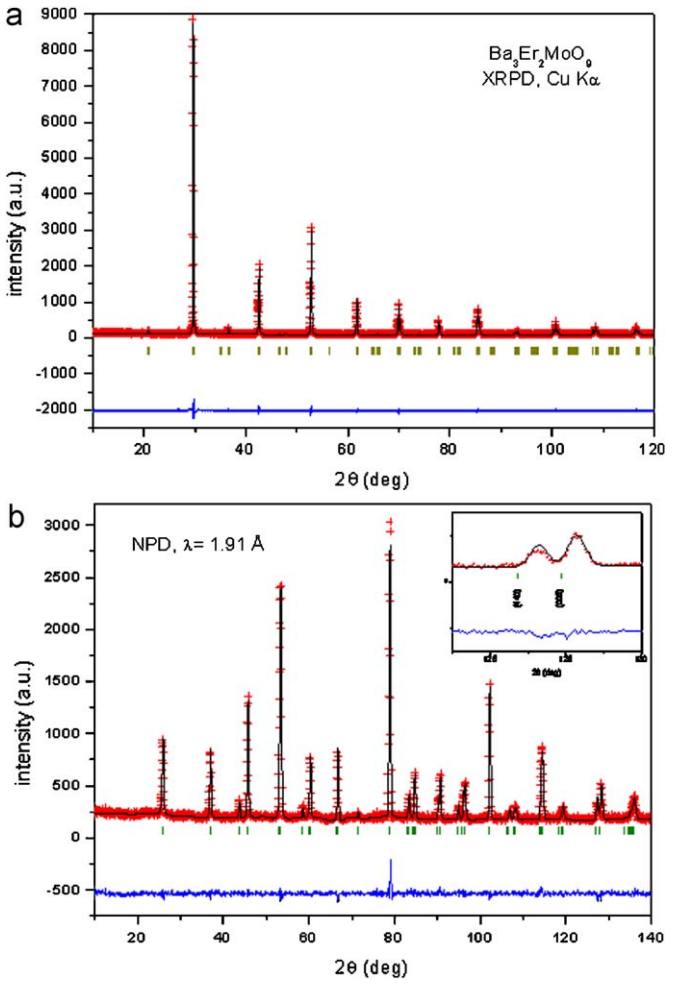

Fig. 2. Observed (circles), calculated (full line) and difference (bottom) profiles after a joint refinement for $Ba_3Er_2MoO_9$: (a) XRPD fit part and (b). High resolution NPD at 295 K fit part. Inset: close up showing the tetrahedral splitting of (440) and (008) reflections.

crystallographic structure and the reliability factors of the two refinements are listed in Table 1; selected angles and main bond lengths are included in Table 2. In Figs. 1 and 2 we show the excellent agreement between observed and calculated profiles after the joint refinements for BHMO and BEMO, respectively. The NPD plots are shown in Figs. 1b and 2b for BHMO and BEMO, respectively.

3.2. Magnetic properties

Fig. 3a and b display the magnetic susceptibility curves of BHMO and BEMO, respectively. Mo(VI) ions are non-magnetic, hence the magnetic behaviour of these compounds is generated only by the lanthanide ions. Both compounds present a paramagnetic behaviour between RT and 3 K at 0.1 T; the reciprocal susceptibility follows a Curie–Weiss law, as shown in the insets of Fig. 3. In Table 3 we present the magnetic parameters obtained from the Curie–Weiss fit for both compounds (see the inset of Fig. 3). *M* vs *H* curves obtained at 3 K are shown in Fig. 4.

3.3. Low temperature NPD

We have carried out NPD measurements in D1B between 275 and 1.8 K for BHMO in order to follow the possible magnetic ordering of the sample. Even at the lowest temperatures we have not observed any magnetic contribution in the low-angle region of the patterns. Although only five reflections are observed in the available angular range, the structure can be successfully fitted to the same space group observed at RT, *I*4/*mcm*, as shown in Fig. 5. The quality of the fit is shown in Fig. 5 for the 1.8 K diagram; Table 4 summarizes the main structural parameters at this temperature. The thermal evolution of the unit-cell parameters and the tilting angle of the HoO_6 and MoO_6 octahedra along the *c*-axis are represented in Fig. 6. The unit cell experiences the expected contraction upon cooling, whereas the octahedral tilting linearly increases when temperature decreases.

Table 1
Unit cell, positional and thermal parameters for $Ba_3Ln_2MoO_9$ (*Ln* = Ho, Er) in the tetragonal *I*4/*mcm* space group, from NPD/XRPD data.

Ln	Ho	Er
$a = b$ (Å)	6.0137(1)	5.9977(3)
c (Å)	8.5477(2)	8.5178(4)
V (Å^3)	309.12(1)	306.41(3)
Ba 4*b*(01/21/4)		
B/Å^2	0.85(4)	0.87(6)
Ln 4*c*(000)		
B/Å^2	0.42(3)	0.60(5)
Occ	0.6667	0.6667
Mo 4*c*(000)		
B/Å^2	0.42(3)	0.60(5)
Occ	0.3333	0.3333
O1 4*a*(001/4)		
B/Å^2	3.0(1)	3.02(2)
O2 8h(*xx*+1/20)		
x	0.2211(3)	0.2247(4)
B/Å^2	2.75(5)	2.355(3)
Reliability factors		
NPD		
R_p (%)	3.08	4.88
R_{wp} (%)	3.82	6.05
R_{exp} (%)	3.77	6.20
χ^2	1.02	0.96
R_B (%)	2.94	5.44
XRPD		
R_p (%)	4.95	5.83
R_{wp} (%)	6.51	7.58
R_{exp} (%)	8.70	7.94
χ^2	0.56	0.91
R_B (%)	3.59	2.62
Global χ^2	1.17	1.57

Table 2
Main interatomic distances (Å) and angles (deg) for $Ba_3Ln_2MoO_9$ (*Ln* = Ho, Er) in the tetragonal *I*4/*mcm* space group from the refinement.

Ln	Ho	Er
BaO_{12}Polyhedra		
Ba–O1 (*x*4)	3.00688(5)	2.9952(3)
Ba–O2 (*x*4)	2.847(1)	2.807(2)
Ba–O2 (*x*4)	3.193(1)	3.160(2)
〈Ba–O〉	3.016	2.987
(*Ln*/Mo)O_6 Octahedra		
(*Ln*/Mo)–O1 (*x*2)	2.13694(4)	2.1295(1)
(*Ln*/Mo)–O2 (*x*4)	2.140(2)	2.131(2)
〈(*Ln*/Mo)–O〉	2.139	2.131
Angles around O		
(*Ln*/Mo)–O1–(*Ln*/Mo)	180.0	180.0
(*Ln*/Mo)–O2–(*Ln*/Mo)	166.81(7)	168.44(9)

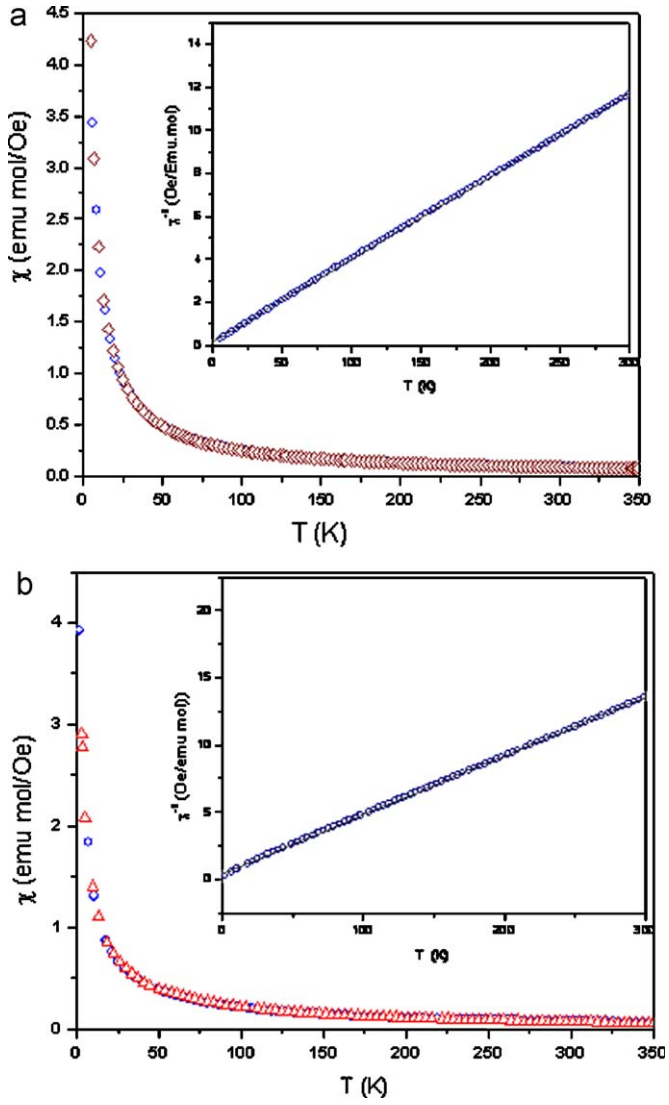

Fig. 3. Magnetic susceptibility thermal variation for (a) $Ba_3Ho_2MoO_9$ and (b) $Ba_3Er_2MoO_9$. At the inset of both parts, figures the Curie–Weiss fits of the inverse susceptibility.

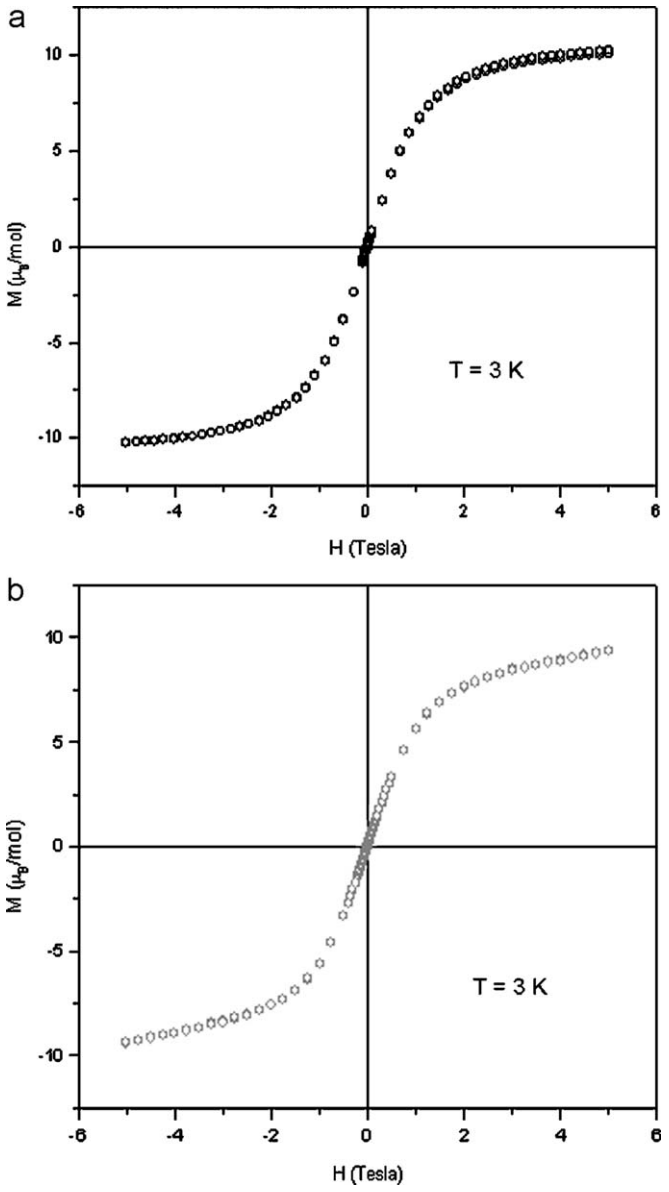

Fig. 4. Magnetization vs magnetic field isotherm ($T = 3$ K) for (a) $Ba_3Ho_2MoO_9$ and (b) $Ba_3Er_2MoO_9$.

Table 3
Constants and Magnetic parameters obtained from the Curie–Weiss fit of the χ^{-1} vs. T curves for BHMO and BEMO.

Ln	Ho	Er
R^2	0.9999	0.9998
θ (K)	−4.74	−9.9
C (emu K/mol)	26.04	21.65
μ_{eff} (μ_B/*Ln*)	10.84	9.9
J	8	9/2
g	1.25	0.75
μ_{calc} (μ_B/*Ln*)	10.61	9.59

Note: $\mu_{calc} = g(J(J+1))^{1/2}$; $\mu_{eff} = 2.83\ C^{1/2}$; $g = 1+\{[S(S+1)-L(L+1)+J(J+1)]/2J(J+1)\}$; $J_{Ho} = L+S$; $J_{Er} = |L-S|$.

4. Discussion

The structure of $Ba_3Ln_2MoO_9$, which should be rewritten as $Ba(Ln_{2/3}Mo_{1/3})O_3$ given the lack of long-range ordering observed between *Ln* and Mo, is defined in the space group *I*4/*mcm*, and can be described as the result of a single anti-phase tilting of the BO_6 octahedra along the *c*-axis. This corresponds to the $a^0a^0c^-$ Glazer's notation, revised by Woodward [12], consistent with the mentioned space group. Fig. 7 illustrates this particular feature. A tilting of 6.6° for *Ln* = Ho and 5.8 for *Ln* = Er at RT can be derived from the *B*–O2–*B* angle. The unit-cell parameters refined for both phases are in agreement with the ionic radii variation of the lanthanide ion, showing BHMO the largest ones. The tetragonal distortion, evaluated as the *a*/*c* ratio [13], takes very similar values for both compounds, 0.703 and 0.704 for BHMO and BEMO, respectively.

The large rare earth cations (i.r. 0.901 and 0.89 Å for Ho and Er, respectively), more usually found at the *A* positions of the perovskite structure, are here occupying, in a large proportion, the *B* positions of the structure. In fact, Goldschmith's tolerance factors (t), were calculated using the ionic radii given by Shannon [14] as $t = (r_A+r_O)/[\sqrt{2}[(2r_{B'}+r_{B''})/3+r_O]]$, adopt values slightly inferior to unity, as 0.968 and 0.972 for BHMO and BEMO, respectively, accounting for their tetragonal symmetry: the previously reported related compounds Ba_2HoMoO_6 and Ba_2ErMoO_6, containing pentavalent Mo cations [15], crystallize in the

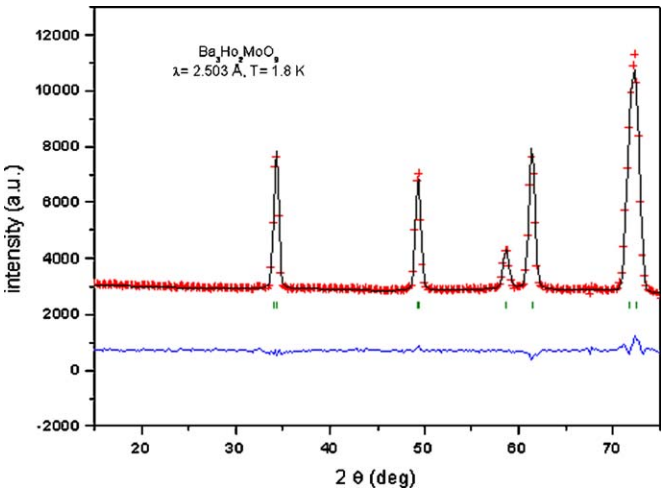

Fig. 5. Observed (circles), calculated (full line) and difference (bottom) profiles after a refinement for $Ba_3Ho_2MoO_9$ from D1B NPD at 1.8 K.

Table 4
Summary of structural parameters for $Ba_3Ho_2MoO_9$ from NPD data at 1.8 K, space group *I*4/*mcm*.

a,*b* (Å)	5.9904(6)
c (Å)	8.543(1)
x(O2)	0.2150(5)
B_{ov}(Å^2)	0.27(1)
χ^2	6.7
R_B (%)	2.7
(Er,Mo)–O1 (Å)	2.1358(3)
(Er,Mo)–O2 (Å)	2.139(3)
(Er,Mo)–O2–(Er,Mo) (deg)	164.1(1)

Ba atoms at 4*b* (0,1/2,1/4); Ho and Mo at 4*c* (0,0,0); (O1) at 4*a* (0,0,1/4); O2 at 8*h* (*x*,*x*+1/2,0) positions.

cubic system space group $Fm\bar{3}m$ (no. 225) and present tolerance factors of 0.987 and 0.989, respectively.

Both perovskites present a complete disordering over the *B* sites of the ABO_3 perovskite. As we have mentioned before, the difference between the neutron scattering lengths of the involved ions are very small, so a joint refinement from high-resolution XRPD and NPD data has been essential for the evaluation of the degree of ordering, taking advantage of the larger contrast existing for X-ray scattering factors combined with the substantial oxygen scattering factor for neutrons, since subtle shifts of oxygen atoms are always associated with ordering–disordering phenomena in perovskites. In a trial refinement in the *I*4/*m* space group, allowing a long-range ordering for Ho and Mo, the degree of *B*-site cations disorder obtained from the refined structures was near to 92% and 95% for BHMO and BEMO, respectively. In fact, the superstructure reflections (e.g. (110) and (113)) are virtually unobservable, and the slight level of ordering determined in *I*4/*m* can be considered an artefact of the refinement; thus we estimate that the description in the *I*4/*mcm* space group is more correct.

If we analyse the combined influence of the charge and the ionic radii difference between two hypothetically different *B*-sites, $(Ln)_{site1}$ and $(Ln_{1/3}Mo_{2/3})_{site2}$, which is the highest degree of ordering that this composition can admit in a double perovskite, we notice that the ionic radii difference is $\Delta r \sim 0.21$ Å and the charge difference between the two sites is 2 ($[3]_{site2a}$–$[5]_{site2b}$); according to these two factors and following the order criterion proposed by Anderson et al. [16], these phases should be ordered.

Another kind of *B* site ordering presented by some double perovskites of formula $A_3B_2'B''O_9$ is the 2:1 ordering. Many of such

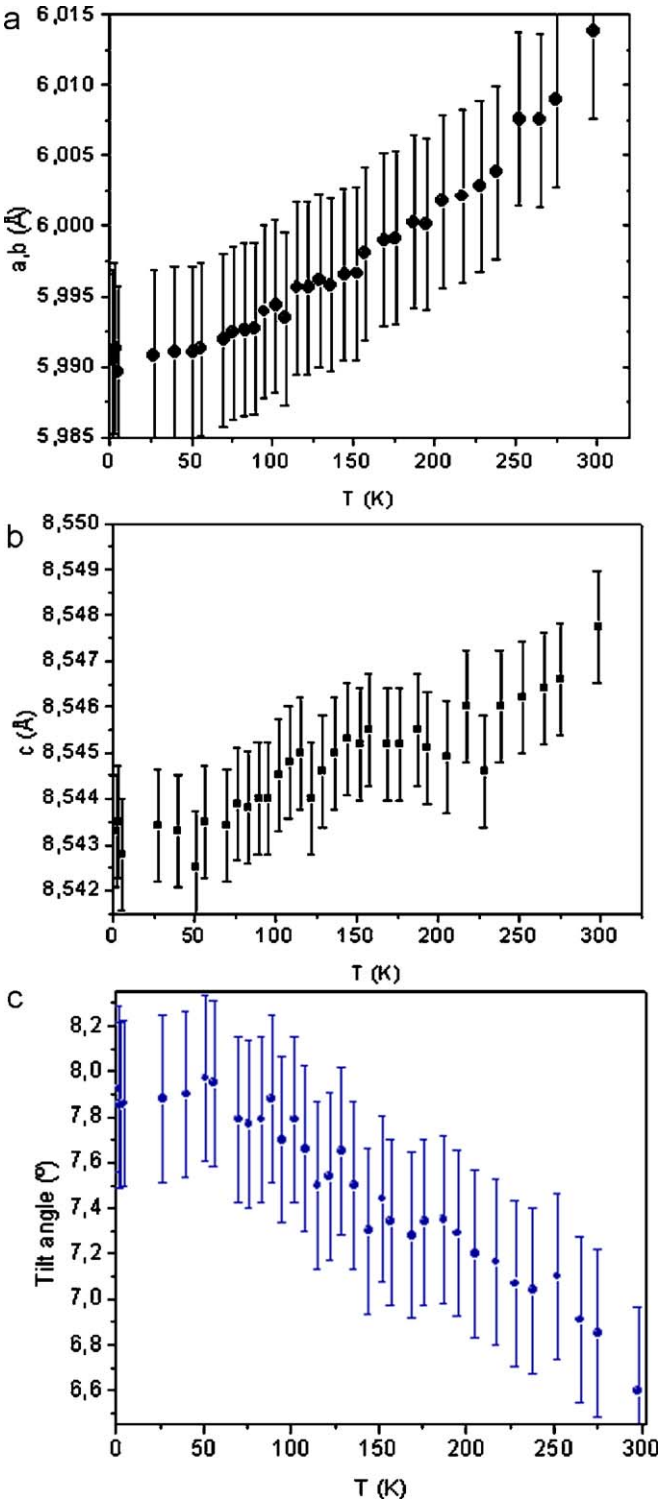

Fig. 6. Thermal evolution between 298 and 1.8 K of (a) *a* and *b* unit cell parameters, (b) *c* parameter and (c) tilting angle of the BO_6 octahedra.

perovskites are known, and the majority of these are hexagonally or trigonally distorted [17]. Generally the most concentrated atom in the formula is a d^0 ion (e.g. Nb^{5+} or Ta^{5+}) that undergoes a second-order Jahn–Teller distortion. The distortion is a response to the presence of two chemically different oxygens (one bound to 2 *B*′ cations, and the other shared by one *B*′ cation and one *B*″ cation) and by this way stabilize the 2:1 ordering system. So d^0 cations (generally the smallest in the structure) almost always

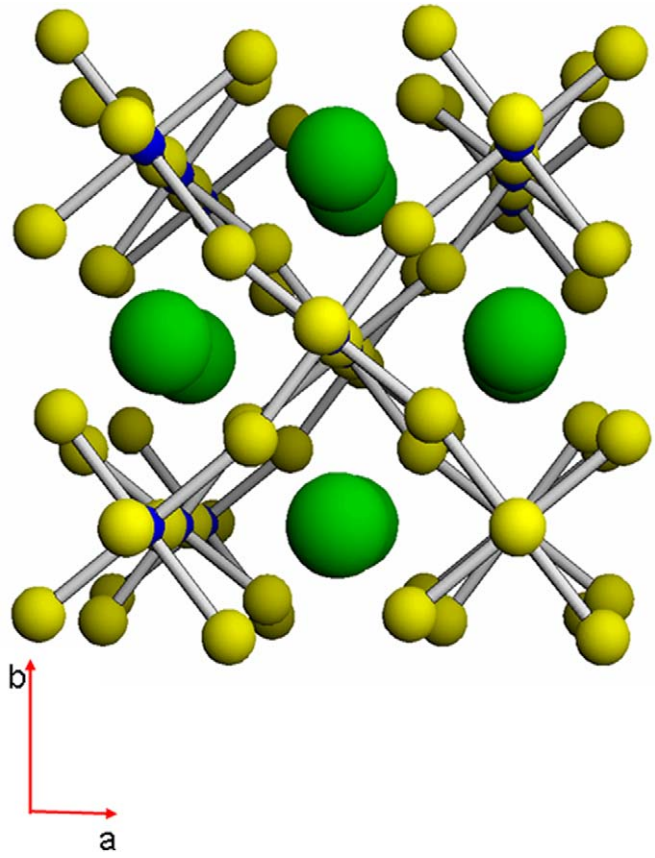

Fig. 7. A projected view of $Ba_3Ln_2MoO_9$ (Ln = Ho or Er) along the (001) direction, where the $a^0a^0c^-$ antiphase rotation of the octahedra is evidenced.

occupy the majority B' sites in 2:1 perovskites, but in our compounds it is Er/Ho rather than Mo^{6+} (d^0 cation) that is the majority cation. Moreover, the tetragonal symmetry observed in the present compounds rules out this type of 2:1 ordering.

As a general fact, the cationic disorder over the B positions in double perovskites generates regions where sets of adjacent highly charged cations give rise to an electrostatic repulsion that promotes the long-range ordering. For the composition $Ba_3Ln_2MoO_9$, the repulsion between highly charged Mo cations is partially shielded by the double contents of Ln^{3+} cations, so disordered structures are obtained. Notice that related compounds such as Ba_2NdMoO_6, containing B' and B'' in a 1:1 ratio, are partially ordered, even if in this case Mo adopts a pentavalent oxidation state [15].

Another interesting structural feature concerns the large thermal isotropic factors observed for the oxygen atoms at RT. Whereas all the metal atoms present reasonable values at RT in the 0.4–0.8 Å^2 range (Table 1), the oxygen atoms at both O1 and O2 positions exhibit abnormally high values of 3.0 and 2.7 Å^2 in BHMO and 3.0 and 2.4 Å^2 in BEMO for O1 and O2. respectively. This can be the result of the large chemical disordering between Ln^{3+} and Mo^{6+} cations, locally requiring very distinct bond lengths, Mo^{6+}–O being strongly covalent whereas R^{3+}–O are fundamentally ionic, thus giving rise to a smearing of the electronic density of the oxygen anions.

The magnetic thermal behaviour of both compounds shows a paramagnetic response of the magnetic susceptibility curves in all the studied temperature range at 0.1 T, and no divergence between the FC and ZFC curves is observed. From the Curie–Weiss fit (see the inset of Fig. 3) we have obtained the parameters that are reported in Table 3. For BHMO (Fig. 3a) the Weiss constant θ obtained was −4.57 K, which is an evidence of weak antiferromagnetic interactions in the paramagnetic state. In addition, the Curie constant obtained was 26.04 emu K/mol, corresponding to an effective paramagnetic moment $\mu_{eff} = 10.84\ \mu_B$/Ho, in excellent agreement with the calculated from $\mu_{calc} = g(J(J+1))^{1/2}$ of 10.61 μ_B. On the other hand, in the case of BEMO (Fig. 3b) the θ obtained was −9.09 K. The Curie constant obtained was 21.65 emu K/mol and the effective paramagnetic moment for Er atom took the value $\mu_{eff} = 9.9\ \mu_B$/Er , which is also in excellent agreement with the theoretical $\mu_{calc} = 9.59\ \mu_B$.

In spite of the presence of weak antiferromagnetic correlations in the paramagnetic regime, the low temperature NPD patterns for the Ho compound do not show any magnetic contribution down to 1.8 K, so we can conclude that no long-range magnetic ordering is reached in the absence of an external magnetic field. However, as illustrated in Fig. 4, M vs H curves at 3 K display a strong polarization of the Ln^{3+} magnetic moments under an external magnetic field. Both curves almost attain saturation for the maximum field of 5 T, reaching magnetization values close to 10 μ_B/f.u. for both perovskites. In any case, it is clear that the direct superexchange interactions between the Ln^{3+} cations via the Ln^{3+}–O1–Ln^{3+} or Ln^{3+}–O2–Ln^{3+} are very weak and they are probably hindered by the complete anti-site disordering exhibited with the Mo^{6+} partners at the B sublattice, leading to a highly frustrated system that does not exhibit any long-range magnetic ordering.

5. Conclusion

A Joint Rietveld Refinement combining XRPD and NPD data has been essential to adequately describe the structure of the phases of stoichiometry $BaLn_{2/3}Mo_{1/3}O_3$, which were formerly described to adopt a cubic or monoclinic symmetry for Ln = Dy. The present study for Ln = Ho, Er shows that they exhibit a tetragonal symmetry (S.G. $I4/mcm$) presenting a total disordering of Ln vs Mo over the B positions of the perovskite. The long-range disorder observed, in spite of the charge differences between Ln^{3+} and Mo^{6+}, is believed to be related to the screening effect of the double contents of Ln^{3+} vs Mo^{6+}. The octahedral framework is tilted in antiphase along the c-axis, with tilt angles of 6.6° and 5.8° at RT for BHMO and BEMO, respectively. A paramagnetic behaviour was identified in the whole temperature range; no magnetic ordering was observed down to 1.8 K by NPD in BHMO. The magnetic moments obtained from the Curie–Weiss Law are in agreement with the theoretical ones and crystal field effects were not observed in the susceptibility curves.

Acknowledgments

S.A.L. thanks a CONICET fellowship. J.C.P. thanks CONICET (Project PIP no. 6246), SECyT-UNSL (Project 7707) and ANPCYT (Project PICT 25459). J.C.P. is a member of CONICET. J.A.A. acknowledges the financial support of the Spanish Ministry of Education to the project MAT2007–60536. We are grateful to I.L.L. for making all facilities available.

References

[1] V. Ting, Y. Liu, R.L. Withers, E. Krausz, J. Solid State Chem. 177 (2004) 979.
[2] R.M. Pinacca, M.C. Viola, J.C. Pedregosa, A. Muñoz, J.A. Alonso, J.L. Martinez, R.E. Carbonio, Dalton Trans. (2005) 447.
[3] R.M. Pinacca, M.C. Viola, J.C. Pedregosa, R.E. Carbonio, J.A. Alonso, J. Mater. Chem. 15 (2005) 4648.
[4] M.S. Augsburger, M.C. Viola, J.C. Pedregosa, R.E. Carbonio, J.A. Alonso, J. Mater. Chem. 16 (2006) 4235.
[5] F. Galasso, L. Katz, R. Ward, J. Am. Chem. Soc. 81 (1959) 820.

[6] F. Galasso, W. Darby, J. Phys. Chem. 66 (1962) 131.
[7] R. Liu, Y. Xuan, Y.Q. Jia, Mat. Chem. Phys. 57 (1998) 81.
[8] M.C. Viola, M.S. Ausburger, R.M. Pinacca, J.C. Pedregosa, R.E. Carbonio, R.C. Mercader, J. Solid State Chem. 175 (2003) 252.
[9] A.F. Fuentes, M. Garza-García, J.I. Escalante-García, G. Mendoza-Suarez, K. Boulahya, U. Amador, J. Solid State Chem. 175 (2003) 299.
[10] S. Oyama, Y. Doi, Y. Hinatsu, Y. Ishii, Bull. Chem. Soc. Jpn. 77 (2004) 1359.
[11] J. Rodríguez-Carvajal, Physica B 192 (1993) 55.
[12] P.M. Woodward, Acta Crystallogr. Sect. B 53 (1997) 32.
[13] D.M. Stein, M.R. Suchomel, P.K. Davies, Appl. Phys. Lett. 89 (2006) 132907.
[14] R.D. Shannon, Acta Crystallogr. Sect. A 32 (1976) 751.
[15] E.J. Cussen, D.R. Lynham, J. Rogers, Chem. Mater. 18 (2006) 2855.
[16] M.T. Anderson, K.B. Greenwood, G.A. Taylor, K.R. Poeppelmeier, Prog. Solid State Chem. 22 (1993) 197.
[17] J.H. Park, P.M. Woodward, Int. J. Inorg. Mater. 2 (2000) 153.